ELSEVIER

Journal of Nuclear Materials 245 (1997) 210–216

journal of nuclear materials

Formation of bubbles in helium implanted 316L stainless steel at temperatures between 25 and 550°C [1]

C.H. Zhang [a,*], K.Q. Chen [a], Y.S. Wang [a], J.G. Sun [b], D.Y. Shen [c]

[a] *Institute of Modern Physics, Academia Sinica, P.O. Box 31, Lanzhou 730000, PR China*
[b] *General Institute for Nonferrous Metals, Beijing 100088, PR China*
[c] *Department of Technical Physics, Peking University, Beijing 100871, PR China*

Received 21 July 1994; accepted 2 January 1997

Abstract

This work studies the formation behavior of helium bubbles in 316L stainless steel implanted with 2.5 MeV He ions at temperatures ranging from 25 to 550°C. The dose and dose rate are 2.5×10^{21} ions/m^2 and $3.2–3.5 \times 10^{16}$ ions/m^2/s for each implantation. Bubble structures in each specimen are investigated with transmission electron microscopy. The temperature dependence of the measured number densities and mean diameters of bubbles exhibits two distinctly different regimes with different apparent activation energies: the regime between 350 and 550°C with high apparent activation energies and the regime between 25 and 350°C with low apparent activation energies. The effect of the pre-implantation cold working is significant on bubble formation only in the regime between 350 and 550°C. Further analysis indicates that the regime between 350 and 550°C is controlled by He diffusion via the self-interstitial/He replacement mechanism and the regime between 25 and 350°C is controlled by He diffusion via the interstitial mechanism. The results are compared with other experimental findings and show consistence with them.

1. Introduction

Previous studies of helium bubble formation in metals found two distinctly different regimes in the temperature dependence of both bubble density and mean size: a high temperature regime characterized by high apparent activation energies and a low temperature regime characterized by low apparent activation energies. The transition occurs around 0.4 of the melting point of metals (in stainless steel around 600°C) [1]. Further analyses indicate that the high temperature regime is gas dissociation controlled whereas the low temperature regime is gas or bubble diffusion controlled [1,2]. Previous efforts to study the underlying mechanisms have focused on the high temperature regime because of some important phenomena such as enhanced swelling in the presence of helium [3] or high-temperature embrittlement resulting from preferential growth of bubbles on grain boundaries [4], while fewer efforts have been paid in the low temperature regime, even for nickel and stainless steels [1]. The lack of data in the low temperature regime has made it impossible to get a clear understanding about fundamental aspects in this regime, such as, the dominant mechanisms for helium diffusion during bubble formation, the significance of bubble migration and coalescence, the effect of concurrent radiation damage on bubble nucleation and growth.

In the present work, formation behavior of helium bubbles in the low temperature regime is studied. Data of bubble densities and mean diameters are analyzed according to the di-atomic nucleation model [5]. Effects of the pre-implantation cold working on bubble formation are also studied.

2. Experimental procedure

The material used for this study is austenitic 316L stainless steel. The composition is listed in Table 1. Two

* Corresponding author. Tel.: +86-931 885 4867; fax: +86-931 888 1100; e-mail: hiam@ns.lzb.ac.cn.

[1] Work is supported by both the Hybrid Reactor Committee and the National Science Foundation of China.

PII S0022-3115(97)00007-X

Table 1
Composition of 316L stainless steel (wt%)

Element	C	Mn	Si	S	P	Mo	Ni	Cr	Fe
Content	0.025	1.41	0.29	0.015	0.017	2.25	14.14	17.22	Balanced

types of the 316L stainless steel with different pre-implantation treatments were used. One was solution annealed at 1050°C for 1 h in a vacuum of 2×10^{-2} Torr. The other was cold-worked to 20% after the same solution-annealing procedure. Specimens of both types were cut into dimensions of 10×5 mm and were well polished to 0.5 mm in thickness.

Helium implantation was performed at a 2×1.7 MV tandem accelerator with 2.5 MeV He^+ beam which produced a uniform dose rate in a 4×4 mm area of a specimen. Specimens were installed in a specimen holder which could be heated with built-in tungsten coils by direct current. The temperature was measured by a thermocouple fixed at the specimen surface. The fluctuation of the temperature was within 15°C during implantation. The charge of the beam was measured with a hollow Faraday cup which was installed in front of the specimen holder. The uncertainty of the measured fluence and flux was within 30%.

Helium implantation was performed at 300, 400, 500 and 550°C, respectively. A solution-annealed and a cold-worked specimen were implanted simultaneously to the same dose level at each temperature. The parameters of the experimental condition are given in Table 2.

After implantation, specimens were electro-plated with nickel in $NiCl_2/NiSO_4$ acid solution to 3 mm in thickness and then were sliced up to make cross-sectional foils. The cross-sectional foils were thinned by ion beam milling and

Table 2
Experimental parameters for each implantation

Fluence (ions/m^2)	Flux (ions/m^2/s)	dpa (max.)	C_{He} (max.) (appm)	P_{He} (max.) (appm/s)
2.5×10^{21}	$3.2–3.5 \times 10^{16}$	9	1×10^5	1.2–1.4

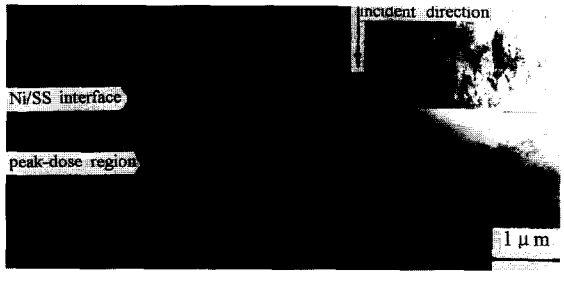

Fig. 1. A typical micrograph of a cross-sectional foils from the solution-annealed specimen implanted at 550°C.

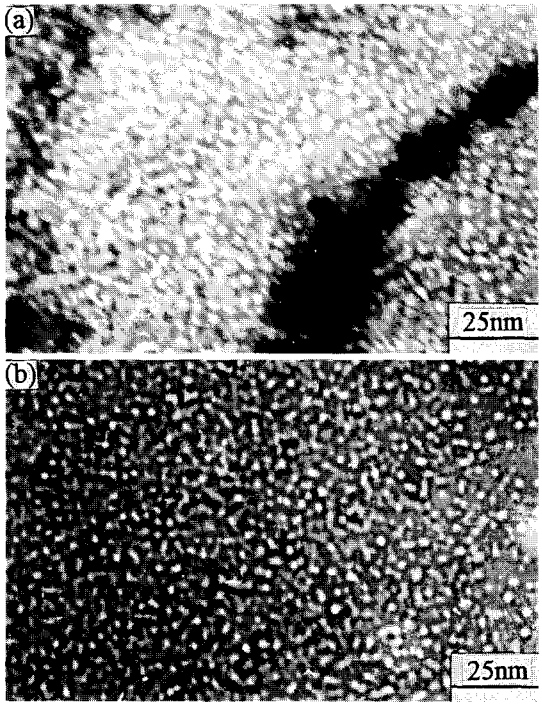

Fig. 2. Typical morphologies of bubbles in the peak-dose region in (a) the solution-annealed specimen and (b) the cold-worked specimen implanted at 300°C.

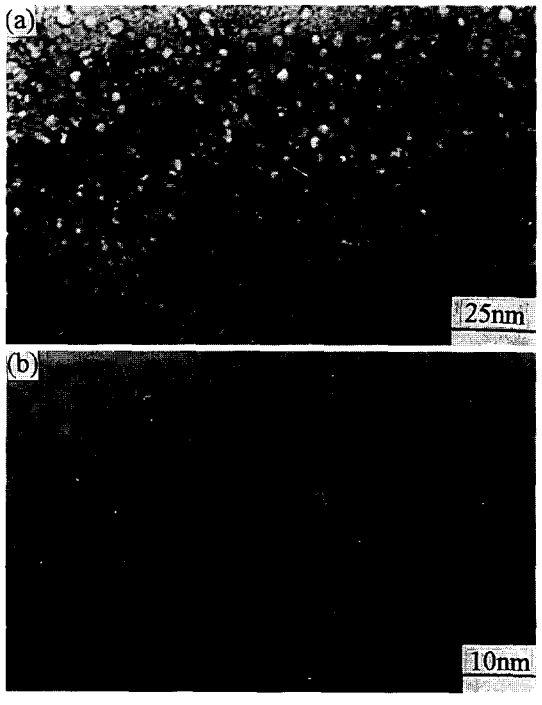

Fig. 3. Typical morphologies of bubbles in the peak-dose region in (a) the solution-annealed specimen and (b) the cold-worked specimen implanted at 400°C.

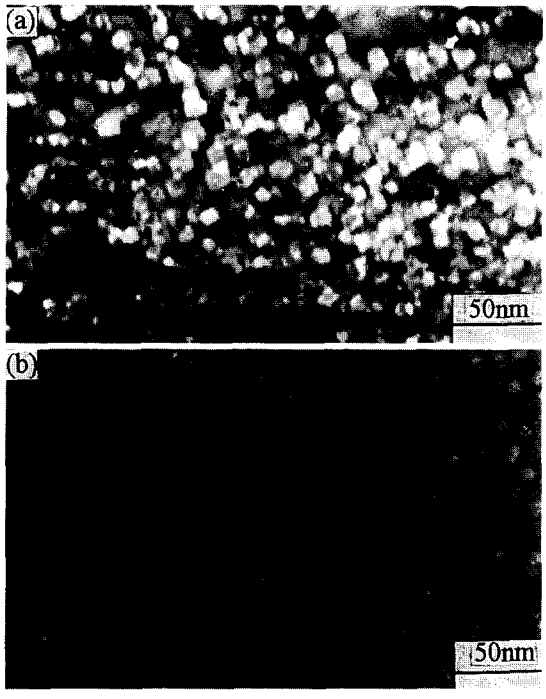

Fig. 4. Typical morphologies of bubbles in the peak-dose region in (a) the solution-annealed specimen and (b) the cold-worked specimen implanted at 500°C.

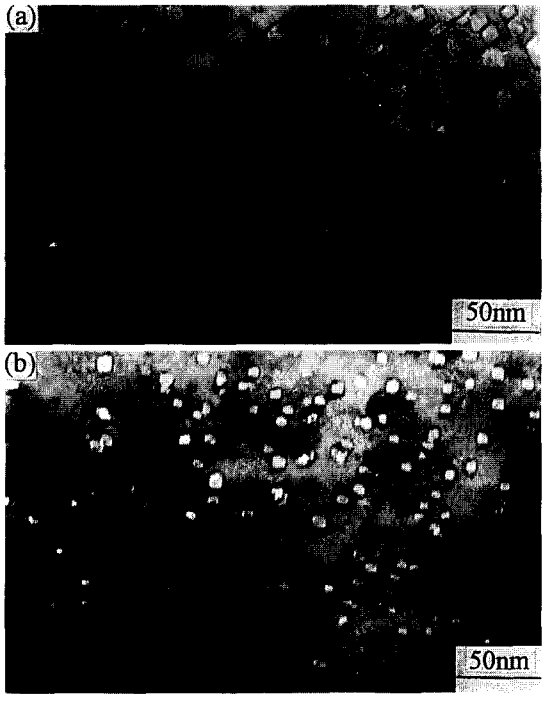

Fig. 5. Typical morphologies of bubbles in the peak-dose region in (a) the solution-annealed specimen and (b) the cold-worked specimen implanted at 550°C.

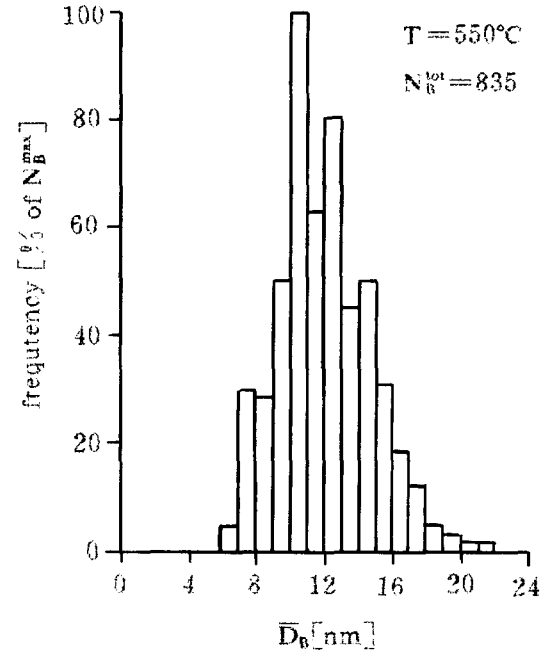

Fig. 6. The size distribution of bubbles in the solution-annealed specimen implanted at 550°C. N_B^{tot} is the number of counted bubbles and N_B^{max} is the number of bubbles in the class with the highest frequency.

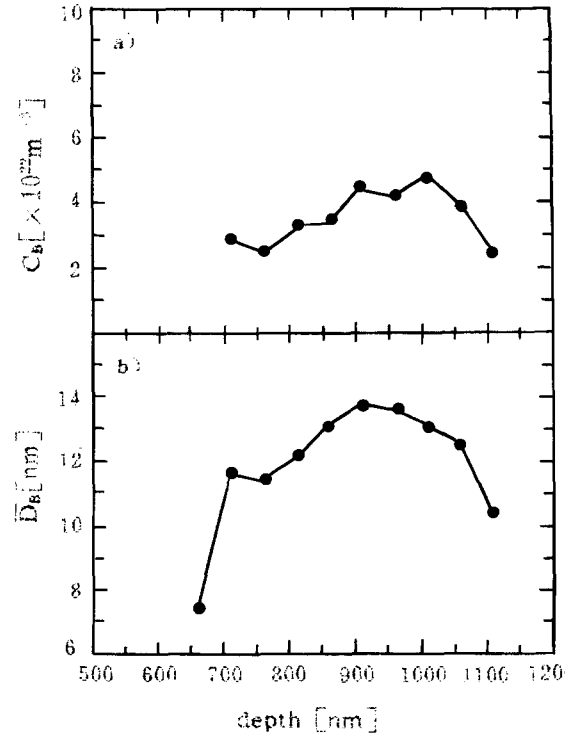

Fig. 7. The cross-sectional profiles of (a) number density and (b) mean diameter of bubbles in the solution-annealed specimen implanted at 550°C.

were investigated in a transmission electron microscope of JEM-200FX. Foil thickness was determined according to diffraction fringes of electron beam on the wedge foils. Number densities and mean diameters of bubbles at different depth along the ion-incident direction were determined manually from the micrographs. About 100 to 300 bubbles were counted at each depth (50 nm interval) along the incident direction. The relative uncertainties for measured bubble densities were within 30% and the absolute uncertainties for mean bubble diameters were within 1 nm.

3. Experimental results

A typical cross-sectional morphology of a foil is shown in Fig. 1. The black band in the matrix which is parallel to the Ni/SS interface is the peak-dose region where most of the implanted helium stopped. Figs. 2–5 show typical morphologies of bubbles in the peak-dose region in each specimen. It is obvious that bubble structures change with temperature as well as pre-implantation treatment. Figs. 6 and 7 show the size distribution and the cross-sectional

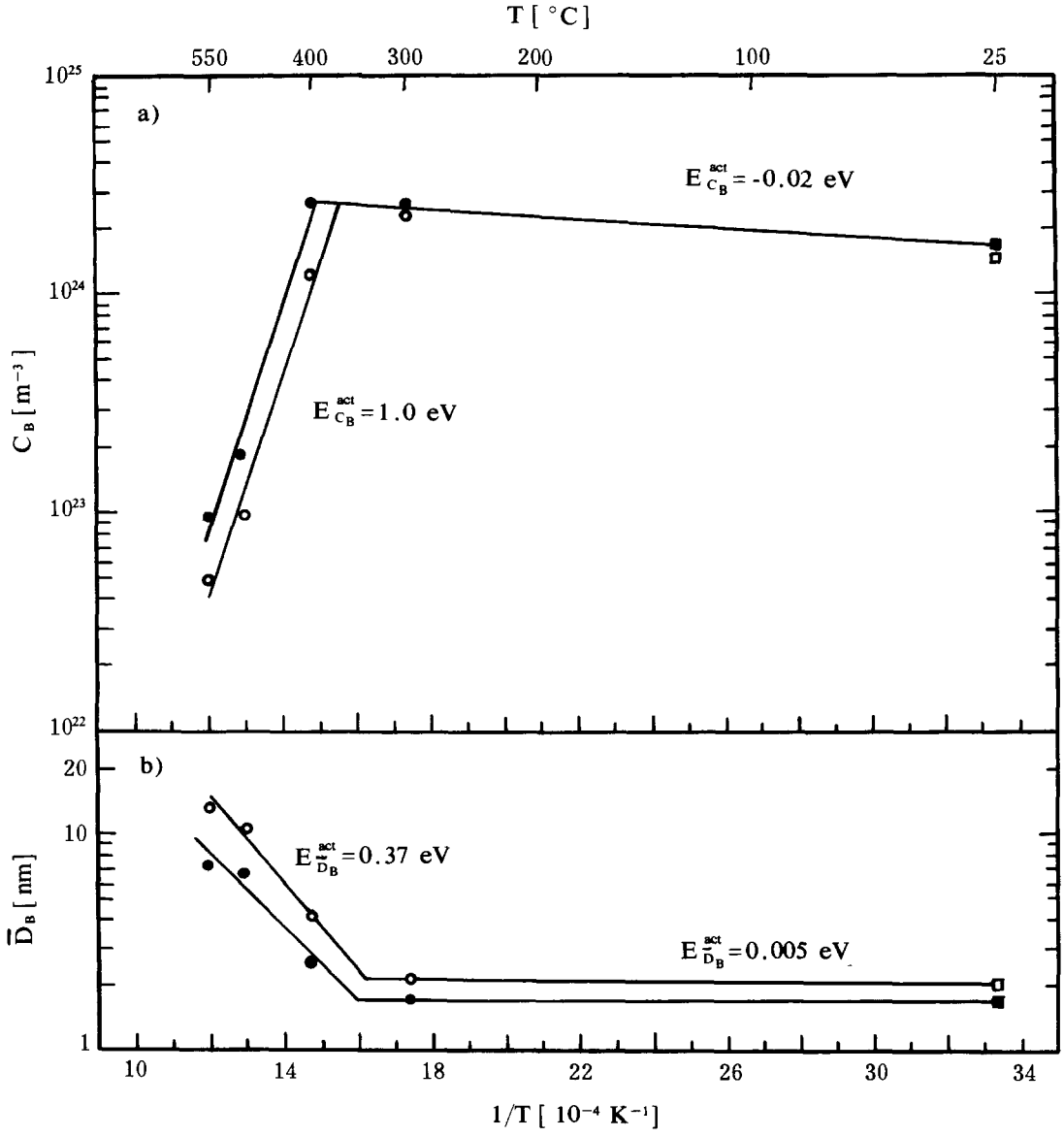

Fig. 8. Temperature dependence of (a) number densities and (b) mean diameters of bubbles in peak-dose region of specimens. The open symbols refer to data points from solution-annealed specimens and the full symbols refer to cold-worked specimens, where ○● refer to the present results, and □ ■ refer to our previous results [7].

profiles of number density and mean diameter of bubbles in the solution-annealed specimen implanted at 550°C. It is found that the size distribution is monomodal, the density and mean diameter of bubbles change with depth. Because different depth along the ion-incident direction corresponds to different concentration of helium or dpa level, the depth dependence of the measured bubble densities and mean diameters would reflect the dose dependence of bubble evolution. However, the diffusion of helium along the concentration gradient would result in significant deviation of the actual helium concentration from the theoretical value given by TRIM calculation, especially at the depth shallower than the peak-dose region at elevated temperatures [6]. Therefore, only data of bubbles in the peak-dose region in each specimen are used in the following analysis. These data and the data from our previous implantation at 25°C [7] are plotted as a function of temperature in Fig. 8.

In Fig. 8 two well-distinct regimes can be distinguished for both C_B and $\overline{D}_B$. The transition occurs around 350°C.

The mean values of the apparent activation energies, when fitting the different branches to an Arrhenius behavior, are as follows.

In the regime between 350 and 550°C

$$E_{C_B}^{\mathrm{act}} = 1.0\ \mathrm{eV}, \qquad E_{\overline{D}_B}^{\mathrm{act}} = 0.37\ \mathrm{eV}. \tag{1}$$

In the regime between 25 and 350°C

$$E_{C_B}^{\mathrm{act}} = -0.02\ \mathrm{eV}, \qquad E_{\overline{D}_B}^{\mathrm{act}} = 0.005\ \mathrm{eV}. \tag{2}$$

It is noticeable that the difference in bubble density between two pre-implantation treatments is very little in the regime between 25 and 350°C, while bubble density in cold-worked specimens becomes significantly higher than in solution-annealed specimens in the regime between 350 and 550°C, which will be discussed later.

4. Discussion

According to previous theoretical work, a bubble nucleus composed of two helium atoms is quite stable, i.e., di-atomic nucleation in the low temperature regime (below 600°C for stainless steels), bubble formation is thus diffusion-controlled [1,5]. For negligible mobility of bubble nucleus the dependence of C_B and $\overline{D}_B$ upon He production rate P_{He} and effective He diffusion constant $D_{\mathrm{He}}^{\mathrm{eff}}$ is as follows:

$$C_B \propto \left(P_{\mathrm{He}}\left(D_{\mathrm{He}}^{\mathrm{eff}}\right)^{-1}\right)^{\alpha}, \qquad \overline{D}_B \propto \left(P_{\mathrm{He}}^{-1} D_{\mathrm{He}}^{\mathrm{eff}}\right)^{\beta}, \tag{3}$$

where the exponents α, β vary with the state of bubbles. For two limiting cases: (1) equilibrium bubbles containing ideal gas, $\alpha = 1/2$, $\beta = 1/4$ and (2) non-equilibrium bubbles containing gas with constant density, $\alpha = 3/7$, $\beta = 1/7$. Accordingly, the apparent activation energies for C_B and $\overline{D}_B$ are as follows:

$$E_{C_B}^{\mathrm{act}} = \alpha E^M, \qquad E_{\overline{D}_B}^{\mathrm{act}} = \beta E^M, \tag{4}$$

where E^M is the effective energy of helium diffusion which varies for different mechanisms of helium diffusion. The proper form of $D_{\mathrm{He}}^{\mathrm{eff}}$ for various mechanisms of He diffusion has been discussed in detail elsewhere [5,8,9]. The apparent activation energies for three typical mechanisms are summarized in Table 3 as predicted by the theories [2,5].

4.1. Bubble formation in the regime between 350 and 550°C

In this regime, our apparent activation energies given in Eq. (1) are found to be consistent with He diffusion via the self-interstitial/He replacement mechanism in the case of equilibrium bubbles (where $\alpha = 1/2$, $\beta = 1/4$) and substantially above the ones for helium diffusion via the vacancy mechanism or the interstitial mechanism as predicted in Table 3, indicating bubble formation is limited by the replacement mechanism in this regime. Helium diffusion via the replacement mechanism has also been identified to control bubble formation in He-implanted Ni [2].

Since our apparent activation energy for C_B is a bit higher than the theoretical value given in Table 3, possibilities are laid open for processes such as bubble migration and coalescence which would result in reduction in bubble density and result in increment in apparent activation energy [10]. Here we would like to discuss another possible process, i.e., thermal instability of di-atomic nuclei of bubbles at temperatures near the transition from the di-atomic nucleation regime to the multi-atomic nucleation regime controlled by He dissociation from bubbles [11]. According to previous computer simulation using various atomic potentials, the binding energy of helium within bubbles would decrease with decreasing size of bubbles especially in the range below 10 helium atoms, the value would be 0.2–0.4 eV for di-atomic nucleus [12,13]. Considering the thermal dissociation of di-atomic nucleus at temperatures near the transition, the apparent activation energy for C_B would be

$$E_{C_B}^{\mathrm{act}} = E_b + \alpha E_V^M, \tag{5}$$

Table 3
Apparent activation energies for three typical mechanisms of helium diffusion, where $E_{\mathrm{V}}^{\mathrm{M}}$ is the energy of vacancy migration, $E_{\mathrm{I}}^{\mathrm{M}}$ is the energy of interstitial migration of helium, $E_{\mathrm{V}}^{\mathrm{M}} = 1.3$ eV, $E_{\mathrm{I}}^{\mathrm{M}} = 0.15$ eV for 316L SS. For two limiting cases: (1) equilibrium bubbles containing ideal gas, $\alpha = 1/2$, $\beta = 1/4$; (2) non-equilibrium bubbles containing gas with constant density, $\alpha = 3/7$, $\beta = 1/7$

	$E_{C_B}^{\mathrm{act}}$	$E_{\overline{D}_B}^{\mathrm{act}}$
Self-interstitial/He replacement mechanism	$\alpha E_{\mathrm{V}}^{\mathrm{M}}$	$\beta E_{\mathrm{V}}^{\mathrm{M}}$
Vacancy mechanism	$\alpha E_{\mathrm{V}}^{\mathrm{M}}/2$	$\beta E_{\mathrm{V}}^{\mathrm{M}}/2$
Interstitial mechanism	$\alpha E_{\mathrm{I}}^{\mathrm{M}}$	$\beta E_{\mathrm{I}}^{\mathrm{M}}$

where E_b is the binding energy for di-atomic nucleus. Good agreement is found between the value of apparent activation energy given in Eq. (5) and our data. Our recent numerical calculation also indicated that including thermal-dissociation term in the rate equations would result in increments in the apparent activation energies [14].

Since in this regime $C_B/P_{He}^{1/2}$ and $\bar{D}_B \cdot P_{He}^{1/4}$ are expected to be independent of P_{He}, we normalize our data of C_B and $\bar{D}_B$ and for comparison, data from other implantation [15] to a He production rate of 1 appm/s. The results are plotted in Fig. 9 and the corresponding implantation conditions are listed in Table 4. It is obvious in Fig. 9(a) that the data band of C_B indeed narrows down substantially by this normalization procedure, indicating the mechanism underlying bubble nucleation is the same for the different implantation conditions with dose varying from 195 appm to 10^5 appm He. The data band of bubble size in Fig. 9(b), however, doesn't narrow down by this normalization procedure, indicating bubble growth is still limited by other parameters such as dose (He concentration as well as dpa level) besides the He production rate and the effective He diffusion coefficient.

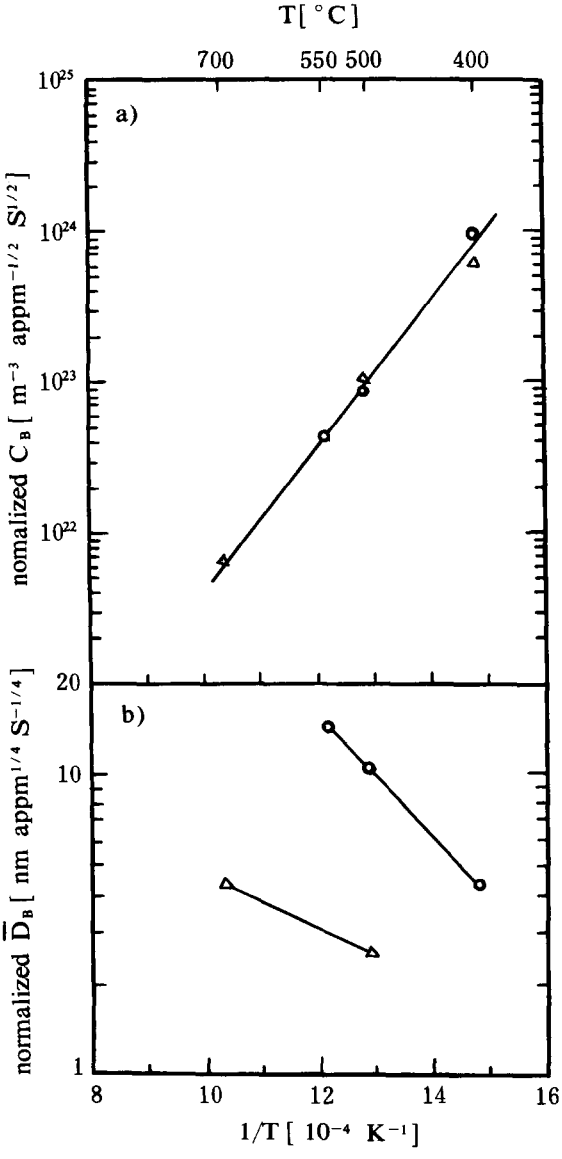

Fig. 9. Temperature dependence of (a) number densities and (b) mean diameters normalized to He production rate $P_{He} = 1$ appm/s according to di-atomic nucleation model. ○ refer to data points from solution-annealed specimen in our work, and △ refer to data points in the work of Choyke et al. [15].

Table 4
List of experimental conditions for data presented in Fig. 9

Key	Material	P_{He} (appm/s)	C_{He} (appm)	dpa	Ref.
△	304 SS	0.013	195	3	[15]
○	316L SS (SA)	1.3	1×10^5	9	our work

4.2. Bubble formation in the regime between 25 and 350°C

In this regime, the limited number and accuracy of data points hamper a detailed analysis. While the very small apparent activation energies for both C_B and $\bar{D}_B$ may favor the helium diffusion via interstitial mechanism according to Table 3. For the ion implantation associated with production of large amount of point defects in the material, helium diffusion via the interstitial mechanism will not dominate if the replacement mechanism is not suppressed efficiently. We may assume that the trapping of helium to vacancies or vacancy clusters is so strong in this temperature regime that He atoms lose their mobility as soon as they are trapped. Accordingly, only a small amount of the implanted helium would participate in the formation of bubbles via the interstitial migration which range is limited crucially by the highly-dispersed vacancies or vacancy clusters, while a large amount of the implanted helium would be trapped in submicroscopic vacancies or vacancy clusters and lose their mobility. Such an interpretation is favored by other two evidences. First, it is found that in this regime there is little difference in bubble density between two pre-implantation treatments: solution-annealing and cold-working (see Fig. 8), indicating the long-range transportation of helium via the replacement mechanism or the vacancy mechanism is suppressed efficiently, to the dislocations which were introduced by cold working, thus the enhancement of bubble nucleation by dislocations is insignificant because of the existence of strong trapping of helium in matrix. Second, the previous positron annihilation study of annealing behavior of helium-implanted Ni shows that there is a plateau stage in the temperature dependence of lifetime components in the

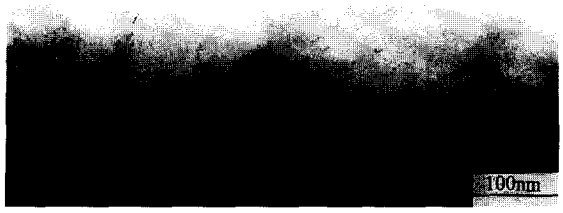

Fig. 10. A typical morphology of bubbles on dislocations in solution-annealed specimen implanted at 550°C.

range below 500°C [16], indicating bubbles as well as submicroscopic vacancy clusters are quite stable in this regime, the later would be strong traps resisting long-range transportation of helium.

4.3. Effect of pre-implantation treatment on bubble formation

In Fig. 8, the difference in bubble density between two pre-implantation treatments: solution-annealing and cold-working treatment is quite little in the regime between 25 and 350°C where bubbles are observed to be homogenous in matrix, while bubble densities in cold-working specimens are significantly higher than in solution-annealed specimens in the regime between 350 and 550°C where the preferential nucleation of bubbles are found on dislocations (see Fig. 10). The difference in the effect of dislocations on bubble nucleation between the two regimes may reflect the different characteristics of two diffusion mechanisms: in the higher temperature regime the long-range diffusion of helium via the replacement mechanism would increase trapping possibility of helium on dislocations, therefore the nucleation of bubbles on dislocations would increase and made bubble density in cold-worked specimen higher than in solution-annealed specimen; while in the lower temperature regime the short-range diffusion of helium via the interstitial mechanism would decrease substantially trapping possibility of helium on dislocations thus prevent nucleation of bubbles on dislocations, as a result, there would be insignificant difference in bubble density between two pre-implantation treatments. Such an explanation is in consistency with the arguments made in Section 4.1 and Section 4.2.

5. Conclusions

In the range between 25 and 550°C, the temperature dependence of number densities and mean diameters of bubbles in helium-implanted 316L stainless steel exhibits two distinctly different regimes with transition occurring around 350°C. The apparent activation energies provide evidence that bubble formation in the regime between 350 and 550°C is controlled by He diffusion via the self-interstitial/He replacement mechanism and the regime between 25 and 350°C is controlled by He diffusion via the interstitial mechanism. Good correlation is found in bubble density between our result and others result after normalization procedure according to the standard di-atomic nucleation model, indicating the mechanism underlying bubble nucleation is the same for different conditions. In the regime between 25 and 350°C, effects of dislocations on bubble formation is insignificant because long-range transportation of helium to dislocations is suppressed efficiently by strong trapping of helium in vacancies or vacancy clusters, while in the range between 350 and 550°C the nucleation of bubbles is enhanced significantly in cold-worked specimens because of the significant long-range transportation of helium to dislocations via self-interstitial/He replacement mechanism and preferential nucleation of bubbles there.

References

[1] B.N. Singh, H. Trinkaus, J. Nucl. Mater. 186 (1992) 153.
[2] V. Zell, H. Schroeder, H. Trinkaus, J. Nucl. Mater. 212–215 (1994) 358.
[3] K. Farrell, P.J. Maziasz, E.H. Lee, L.K. Mansur, Radiat. Eff. 78 (1983) 277.
[4] H. Ullmaier, Radiat. Eff. 78 (1983) 1.
[5] H. Trinkaus, J. Nucl. Mater. 133&134 (1985) 105.
[6] P.X. Wang, Y.P. Li, J.R. Liu, G.G. Zhang, R.Z. Ma, P.R. Zhu, C. Qiu, T. Xu, J. Nucl. Mater. 169 (1989) 167.
[7] K.Q. Chen, S.H. Yang, Z.G. Wang, J.G. Sun, J.M. Quan, L.W. Li, Y.M. Sun, J. Nucl. Mater. 191–194 (1992) 737.
[8] H. Trinkaus, J. Nucl. Mater. 118 (1983) 39.
[9] N.M. Ghoniem, S. Sharafat, J.M. Williams, L.K. Mansur, J. Nucl. Mater. 117 (1983) 96.
[10] M. Fell, S.M. Murphy, J. Nucl. Mater. 172 (1990) 1.
[11] H. Trinkaus, Radiat. Eff. 78 (1983) 189.
[12] J.Th.M. De Hosson, L. Caspers, A. van Veen, Radiat. Eff. 78 (1983) 25.
[13] W.D. Wilson, C.L. Bisson, M.I. Baskes, Phys. Rev. B24 (1981) 5616.
[14] C.H. Zhang, K.Q. Chen, Y.S. Wang, J.G. Sun, in: Proc. 3rd Sino-Japanese Symp. Materials for Advanced Energy Systems and Fission and Fusion Engineering, Chengdu, China, Oct. 29th–Nov. 3rd, 1995, eds. D. Xiwen et al., p. 230.
[15] W.J. Choyke, J.N. Mcgruer, J.R. Townsend, J.A. Spitznagel, N.J. Doyle, F.J. Venskytis, J. Nucl. Mater. 85&86 (1979) 647.
[16] D. Segers, L. De Schepper, D. Geshef, L. Dorikens-Vanpraet, M. Doriken, J. Paridaens, G. Severne, L.M. Stals, Mater. Sci. Forum 105 (1992) 1221.